

CARMA Memorandum Series #20
**Version 2 CARMA Configurations for
Cedar Flat**

Tamara T. Helfer
Radio Astronomy Lab, UCB
February 4, 2004

ABSTRACT

This report presents a revision of the Version 1 Cedar Flat CARMA configurations given by Helfer & Wright in April 2003. The 15-element configurations in this report take into account specific characteristics and limitations of the Cedar Flat site. Here, a complete set of five CARMA configurations is presented, with baselines as long as 1.9 km for A array and as short as 8.3 m for the most compact E array. The resolution scale factor between adjacent arrays is 2.5 for all but the two most compact arrays, where it is 2.0 (in order to allow for relatively short baselines for the D array). A total of 60 stations is needed to populate the five arrays. A corrected treatment of the issue of shadowing for the compact arrays is also presented. The orientation of the E array has been optimized with regard to shadowing properties; furthermore, for this array, the shadowing is nearly identical for the cases where the current relative heights of the BIMA and OVRO elevation axes are preserved and where the BIMA antennas are instead lowered by 0.5 m. The elevations of all the proposed pads on the Cedar Site change by less than 50 m over the 2 km extent of the arrays, and the effect of the elevation differences on the uv coverages and synthesized beams is trivial.

Change Record

Revision	Date	Author	Sections/Pages Affected
Remarks			
1.0	2003-Aug-20	T.T. Helfer	Original version, submitted to CARMA Memo series on 2004-Feb-04.

1. Introduction

Following the presentation of a set of six configurations for the Cedar Flat site (the “Version 1” configurations, Helfer & Wright 2003), Glen Petitpas (UMD) and Tony Beasley (OVRO) went to the site and investigated the proposed pad locations, paying particular attention to accessibility, visibility (of and from the antennas) and local ground characteristics. Their most severe findings were that some of the proposed A and B array locations were inaccessible and/or had poor visibility at low antenna elevations.

Other CARMA members also offered feedback on the Version 1 configurations. The main suggestions were (1) to make the resolution scale factor (RSF) between adjacent arrays more uniform; (2) to investigate the possibility of eliminating one of the intermediate arrays; (3) to make sure that each antenna in the most compact array had a “safe” location where it could be parked while the rest of the array was allowed to operate; and (4) to continue to try to keep the total number of pads as small as practical.

Based on these considerations, I have designed a revised set of five CARMA configurations for the Cedar Flat site. The array characteristics are described below. As with the Version 1 document, these configurations use six 10.4 m OVRO antennas and nine 6.1 m BIMA antennas, and I defer consideration of the 3.5 m SZA antennas.

2. Optimization for Beam Elongation

The configurations were designed with the help of Boone’s optimization code (Boone 2001, 2002) as described in the Version 1 document. The Boone optimization allows the user to specify the source declination at which round beams are desired. By judicious selection of this parameter, it is possible to achieve beam elongations $\theta_{maj}/\theta_{min}$ that are relatively round for the greater portion of the sky. As the top panel of Figure 1 shows, for an optimized declination of $\delta_{opt} \sim 5^\circ$, the resulting beams are elongated less than $\sim 20\%$ for sources at declinations from about -10° to $+80^\circ$. For source declinations below $\delta \lesssim -10^\circ$, the beams become progressively elongated when $\delta_{opt} \gtrsim 5^\circ$; at an extreme, when $\delta = -30^\circ$, $\theta_{maj}/\theta_{min} = 2.1$ for $\delta_{opt} = 5^\circ$, and $\theta_{maj}/\theta_{min} = 2.5$ for $\delta_{opt} = 50^\circ$.

All arrays were therefore optimized for round beams at declination $\delta_{opt} = 5^\circ$. The resulting elongations for the Version 2 arrays are shown in the bottom panel of Figure 1. Since the B array was constrained to share 6 antennas with the A array, and since it was constrained by the site mask, the B array turns out to have its roundest beams at about $\delta = 0^\circ$, even though I specified a source declination of $\delta_{opt} = 5^\circ$. Still, the peak elongation of the B array is only about 26% over the range from $\delta = -10^\circ$ to $+85^\circ$.

3. Configuration Evaluation

I evaluated the configurations based on both objective and subjective criteria. The chief objective criteria were the rms, maximum and minimum sidelobe levels measured over the central $\sim 14 \times 14$ beamwidths for each array, where a gaussian had first been fitted and removed from the central lobe.¹ The subjective criteria included inspections of the plots of uv coverage and histograms of the radial uv density. Here, I was chiefly concerned that the uv coverage was relatively uniform and that there were no egregious gaps in coverage, especially at short spacings, where the Boone algorithm often does not perform well (Helfer & Wright 2003). Another important subjective criterion was inspection of the synthesized beam images for non-gaussian shapes at low levels in the central lobe. It turned out to be fairly common to get beams with low near-in sidelobe levels that nonetheless had wings, “ears”, or other irregular shapes attached to the central lobe at the ~ 5 – 10% level. Since these low-level beam structures might be problematic to clean and remove from non-ideal observations, I discarded such beams even if it meant choosing an array with somewhat higher overall sidelobe levels.

Although the Boone code is an optimization algorithm, its results are not unique solutions to configuration design. In practice, it is possible to generate different optimized arrays with very similar properties given different initial configurations. I therefore typically ran many different optimizations for each array, specifying different initial conditions each time. For each set of initial conditions, I also ran each optimization for three to six iterations in order to test the convergence of the solution. Often, an intermediate iteration yielded the best solution for a given configuration.

4. The Configurations

A new complete set of five configurations for Cedar Flat is shown in Figure 2, where shared stations are indicated by multiple symbols. The configurations are designated by the letters A (largest) through E (smallest). The four A–D configurations are also shown together on a masked topographical map of the site in Figure 3, using the same symbols as in the previous figure. The A, B, and C stations are shown overlaid on a detailed topographical map in Figure 4. The station positions for all arrays are listed in Table 1, in meter offsets relative to the 0,0 position, defined to be at latitude = $37^\circ 16' 43''$ N, longitude = $118^\circ 08' 32''$ W.

¹The sidelobe levels at large distances from the central lobe are determined largely by the number of antennas and are nearly independent of the specific array design.

The site elevations at each pad location, taken from U.S. Geological Survey (USGS) digital elevation models, are also given in Table 1.

Following optimization with Boone’s code, I moved some individual pads by small amounts to accommodate shared stations with other arrays. In general, it did not prove to be fruitful to re-optimize the arrays after such moves.

The site mask used here (Figure 3, excluding archeological sites) was based on input from Petitpas and Beasley and is much more restrictive than what was used earlier. I fixed the four A array stations west of Rte 168 (the main North-South road in Figure 4) based on input from Beasley, and we also fixed the A array station at (E,W)=(-552m,-583m), just east of Rte 168 near the southern end of the loop road. I was then able to iterate to place two additional A array pads along the southern part of the loop road, and to place another two shared A/B array pads just west of the loop road. An additional shared A/B pad lies along the existing north-south camp road shown in Figure 4. By placing antennas along these existing roads, we can hope to see a significant savings on site development costs for CARMA.

Array Placement on the Site and Shared Stations

While the placement of the A and B arrays were more or less centered within the available site mask, Beasley and Petitpas determined that the smaller arrays would do well to be centered somewhat to the east on the site. This keeps most of the CARMA stations away from tall trees and difficult terrain and also away from the creekbed that runs North-South through the heart of the site (Figure 4). Since the C array is therefore considerably offset to the east from the B array, this choice means that there is only one shared station between these two arrays. There are six shared stations between the A and B arrays, four between the C and D arrays, and four between the D and E arrays, for a total of 60 stations for the set of five CARMA configurations. If the C, D, and E arrays were moved further west towards the central part of the B array, it would be possible to share an additional 3 stations. However, site development issues suggest that it is probably is not cost effective to do so.

5. Beam Sizes, Spatial Dynamic Ranges, and Scale Resolution Factors

Sample beams and uv coverages for the five Version 2 arrays are shown in Figures 5 and 6, and histograms of the radial uv densities are shown in Figure 7. The beam sizes and related parameters are listed in Table 2, for $\nu = 230$ GHz and declinations $\delta = 30,0,-30^\circ$. The E array yields naturally-weighted beams of about $4.2''$ at 230 GHz, down to $0.13''$ beams available in A array. The near-in sidelobes have typical rms levels of about 2–3% and peak

near-in sidelobes of about 7% for sources away from the equator.

The beam elongations, spatial dynamic ranges, and resolution scale factors (RSFs) between adjacent arrays are listed in Table 3 for $\nu = 230$ GHz and $\delta = 5^\circ$. The beam elongations (shown in Figure 1 for all source declinations) range from 1.02 to 1.09 for this declination. The ratio of maximum to minimum projected baselines, which is a measure of the spatial dynamic range of the configuration, ranges from about 11 for the A and E arrays to about 17 for the intermediate arrays at this declination. These choices reflect the desire to have the A (E) array be most sensitive to long (short) baselines, with the intermediate arrays stretched to be sensitive to a larger spatial dynamic range.

The RSFs are now fixed at 2.5 between all arrays except the two most compact arrays, where the RSF is 2.0. The choice of a smaller RSF between the E and D arrays allows the D array to have relatively short baselines without having too large a spatial dynamic range (which results in poor uv coverage and beams). The D array has a minimum baseline of 11.0 m, which is somewhat larger than that of the current C array at BIMA, where it is 9.9 m.

The RSFs of 2.0/2.5 compare favorably with the current situation at BIMA, where the RSF is 2.1 between the BIMA D and C arrays, 2.8 between the BIMA C and B arrays, and 7.1 between the BIMA B and A arrays. It also compares well with the current situation at OVRO, where the RSF is 2 between the OVRO Compact and Low arrays and 3 between the OVRO Low and Low+High arrays.

6. Compact Array Design and Shadowing

Compact Array Design

The Version 1 compact array had at its core a set of five closely packed BIMA antennas. These pad locations were designed by John Lugten (UCB) and were placed at the center and near four of the five corners of a regular pentagon. The shortest baselines then occurred between the center and each of the four corners. This placement allowed good uv coverage for the shortest baselines at nearly all azimuths. Unfortunately, subsequent analysis by Matt Fleming (UCB) showed that the central BIMA antenna did not have an acceptable “safe” position, that is, a location where the antenna could be parked without possibility of collision with the other antennas while the rest of the array was allowed to operate.

The compact E array presented here is therefore of a new design. Lugten again designed the central five pads, this time based on a regular 7-sided figure instead of a pentagon. This design has the advantage that the shortest baselines are now between the pads at the corners

of the 7-sided figure instead of between the corners and the center of the figure, which allows all of the antennas to be safely parked. Using these fixed 5 pad locations, I used Boone’s code to optimize the remaining four BIMA antennas and the six OVRO dishes. Here, it was not advantageous to let the optimization code iterate too long, since it tended to move too many OVRO dishes closer than their allowed minimum separation from the other antennas. In the end, after optimization, I had to move two antennas slightly by hand in order to preserve the desired BIMA-OVRO and OVRO-OVRO dish separations.

Shadowing

Antenna shadowing is an issue for CARMA only for low-declination observations of the E array (Table 2)². In the Version 1 document (Helfer & Wright 2003), the shadowing results given for the compact arrays were incorrect. That calculation considered only BIMA-on-BIMA dish shadowing, or geometric shadowing at 6.1 m dish separation. With programming assistance from Peter Teuben (UMD), who wrote a new MIRIAD task called CSFLAG (“CARMA shadowing flag”), I have now corrected this calculation to include BIMA-on-BIMA shadowing, BIMA-on-OVRO/OVRO-on-BIMA shadowing, and OVRO-on-OVRO shadowing, where the shadowing criterion is set to be the sum of the dish radii for any given pair.

After optimization of the E array, I wrote a script to check for the optimal orientation to alleviate shadowing for low declination sources. To do this, I rotated the optimized array in 5° increments, and then stretched the rotated array by 8% in the North-South direction in order to alleviate shadowing at transit and to achieve somewhat rounder beams at $\delta = 5^\circ$. For each orientation, I further examined the cases where the relative heights of the BIMA and OVRO elevation axes differed by up to 1.0 m.

The results of this experiment are shown in Figure 8, which shows shadowing as a function of rotation for sources at $\delta = -5^\circ$ (top) and $\delta = -30^\circ$ (bottom). (These are the declinations of Orion and of the Galactic Center, two popular low-declination sources.) For each plot, the black curve shows the case where the BIMA elevation axis is 0.5 m lower than the OVRO elevation axis, which is the current situation. The red curve shows the case where the BIMA elevation axis has been lowered by an additional 0.5, which has been proposed as a way to provide a more stable mount for the BIMA dishes.

In general, the curves show that the shadowing for this E array will remove 1–6% of the visibilities for sources at Orion’s declination, and shadowing will remove 69–77% of the visi-

²For the CARMA D array, shadowing starts to set in at about $\delta = -20^\circ$, but even by $\delta = -30^\circ$, only 5% of the visibilities from a 4-hour track centered at transit are shadowed (Table 2).

bilities at the Galactic Center. The curves also show a clear preference for array orientations around iteration 6, where the effects of shadowing are minimized. Also, at this orientation, the shadowing is only slightly worse when the height of the BIMA elevation axis is lowered. For the E array, I therefore chose iteration 6, where the shadowing is optimized for both Orion and Galactic Center observations. The E array is shown in Figure 9 with the placements of the BIMA and OVRO dishes.

7. Effect of Site Elevations on Beams

The elevations of the proposed pads on the Cedar Flat site (Table 1) range from 2194 m to 2243 m. For the E/D/C/B/A arrays, the maximum change in pad elevations is 3/5/17/28/49 m over configuration diameters of 66/148/373/942/1880 m. How do the site elevations affect the uv coverages and beams? To first order, the array with the smallest ratio of configuration diameter to elevation change should be the one that is most affected by the nonplanar arrays. For the E/D/C/B/A arrays, this ratio is 22/30/22/34/38. I generated uv coverages and beams for the E array with the correct site elevations (including the 0.5 m difference in elevation height axes) and compared them with those shown in Figure 5 and Table 2, which were generated from planar arrays. The results were nearly identical. The near-in rms sidelobe levels changed by 0.1% or less for $\delta = +30, 0, -30^\circ$, and the uv coverages and synthesized beams were nearly indistinguishable by eye.

8. Conclusions

I have presented a complete set of five configurations for CARMA that take into account specific characteristics and limitations of the Cedar Flat site. I discussed general and specific design considerations as well as how possible configurations were evaluated, and I discussed some of the basic properties of the arrays, including beam characteristics, shared stations, and spatial dynamic ranges. I presented a more extensive discussion of how the most compact array was generated, with special attention to the issue of shadowing.

I thank Tony Beasley, Frederic Boone, Matt Fleming, John Lugten, Glen Petitpas, Dick Plambeck, Peter Teuben, and Mel Wright for their input on this work and for very helpful discussions.

REFERENCES

Boone, F. 2001, *A&A*, 377, 368

Boone, F. 2002, *A&A*, 386, 1160

Helfer, T.T. & Wright, M.C.H.W. 2003, CARMA Memo #19,
<http://www.mmarray.org/memos>, “Version 1” configurations

Table 1. CARMA Stations

East (m)	North (m)	Up (m)	A	B	C	D	E
-1217.10	-136.20	2243	X
-1108.00	883.00	2235	X
-866.00	650.00	2224	X
-810.77	79.64	2218	X
-552.00	-583.00	2211	X
-331.53	56.82	2220	X	X
-310.57	339.88	2222	X	X
-249.90	-789.91	2190	X
-199.09	156.93	2206	...	X
-188.94	697.49	2210	X
-156.50	329.06	2205	...	X
-140.00	-455.37	2193	X
-121.89	443.79	2204	X	X
-115.28	880.39	2215	X
-89.69	216.84	2201	...	X
-79.75	32.69	2199	X	X
-75.31	815.10	2215	...	X
-65.98	114.00	2199	...	X
-11.90	389.98	2202	...	X
-8.62	574.99	2214	...	X
34.37	304.21	2200	X
72.43	385.72	2205	X
73.00	160.79	2196	X
78.95	244.79	2198	...	X	X
96.70	57.95	2194	X
113.85	430.07	2211	X
119.20	283.92	2199	X	...
124.96	271.77	2199	X
130.97	144.86	2196	...	X
134.33	316.31	2201	X	...
134.55	226.93	2198	X	X	...
136.92	260.31	2199	X	...
143.97	186.06	2197	X	...
149.34	286.76	2200	O
150.78	333.93	2202	X	...
156.48	154.17	2196	X
158.55	270.66	2199	X	B

Table 1—Continued

East (m)	North (m)	Up (m)	A	B	C	D	E
159.01	253.21	2198	X	X	...
159.97	307.10	2201	O
167.04	263.72	2199	X	B
167.73	224.30	2198	X	X	...
170.82	274.08	2199	B
176.30	254.15	2198	X	O
177.72	281.53	2199	B
178.57	271.03	2199	X	X	B
185.37	304.45	2200	O
185.72	275.49	2199	B
187.15	284.26	2199	B
190.57	261.97	2199	B
191.19	248.66	2198	O
198.27	274.65	2199	B
201.57	238.04	2198	X	...
202.57	296.20	2200	O
214.02	293.25	2200	X	...
221.49	268.76	2199	X	...
241.64	188.74	2196	X
252.46	-68.05	2194	X	X
267.09	329.15	2200	X
291.78	266.05	2197	X
349.73	500.08	2197	X	X

Table 2. Beam sizes, sensitivities, sidelobes, shadowing, and spatial dynamic ranges at $\nu=230$ GHz for $\delta=30,0,-30^\circ$

Config	δ ($^\circ$)	HA (hrs)	σ (mJy)	$\theta_{maj} \times \theta_{min}$ (")	σ_{Tb} (mK)	Sidelobe rms ^a (%)	... max ^a (%)	... min ^a (%)	Nvis ^b (%)	uv min ^c (m)	uv max ^c (m)
A	30	-2,2,,01	0.23	0.15 x 0.12	295.4	2.9	7.8	-7.0	100	192.9	1881.6
A	0	-2,2,,01	0.27	0.15 x 0.15	277.4	3.3	14.8	-7.1	100	146.1	1827.3
A	-30	-2,2,,01	0.56	0.32 x 0.15	269.7	2.9	8.8	-6.7	100	60.3	1692.3
B	30	-2,2,,01	0.23	0.37 x 0.30	47.9	3.0	9.7	-6.7	100	81.6	942.6
B	0	-2,2,,01	0.27	0.38 x 0.37	44.4	3.3	15.4	-7.1	100	64.8	894.0
B	-30	-2,2,,01	0.56	0.75 x 0.38	45.4	2.9	6.7	-6.6	100	30.6	809.1
C	30	-2,2,,01	0.23	0.90 x 0.75	7.9	2.0	4.4	-5.9	100	24.6	372.6
C	0	-2,2,,01	0.27	0.94 x 0.90	7.4	2.7	15.4	-6.9	100	18.3	322.8
C	-30	-2,2,,01	0.56	1.88 x 0.92	7.5	2.1	6.0	-6.2	100	10.2	279.3
D	30	-2,2,,01	0.23	2.22 x 1.91	1.3	2.2	6.1	-6.1	100	10.2	147.9
D	0	-2,2,,01	0.27	2.39 x 2.22	1.2	2.9	11.5	-6.9	100	7.5	128.1
D	-30	-2,2,,01	0.57	4.74 x 2.25	1.2 ^d	2.1 ^d	7.7 ^d	-6.4 ^d	95	4.5	112.5
E	30	-2,2,,01	0.23	4.48 x 3.94	0.3	2.9	7.8	-6.7	100	7.5	66.3
E	0	-2,2,,01	0.27	4.98 x 4.43	0.3	3.7	21.2	-7.0	100	6.0	64.5
E	-30	-2,2,,01	1.00	7.56 x 3.51	0.9 ^d	4.6 ^d	18.3 ^d	-11.3 ^d	30	3.3	55.5

^aSidelobe rms, max, min measured over central $\sim 14 \times 14$ beamwidths

^bPercentage of unshadowed visibilities for given hour angle range; corrected calculation since Version 1 document

^cProjected minimum and maximum baselines

^dShadowed data have been flagged

Table 3. Beam elongations, spatial dynamic ranges, and RSFs at $\nu=230$ GHz and $\delta=5^\circ$

Config	θ_{maj} (")	θ_{min} (")	$\theta_{maj}/\theta_{min}$	S_{max}/S_{min} ^a	RSF ^b
A	0.148	0.145	1.02	11.7	
B	0.378	0.348	1.09	13.1	B/A=2.48
C	0.898	0.884	1.02	16.8	C/B=2.46
D	2.25	2.21	1.02	16.6	D/C=2.50
E	4.69	4.43	1.06	9.9	E/D=2.04

^aRatio of maximum projected baseline to minimum projected baseline

^bResolution scale factor between adjacent arrays

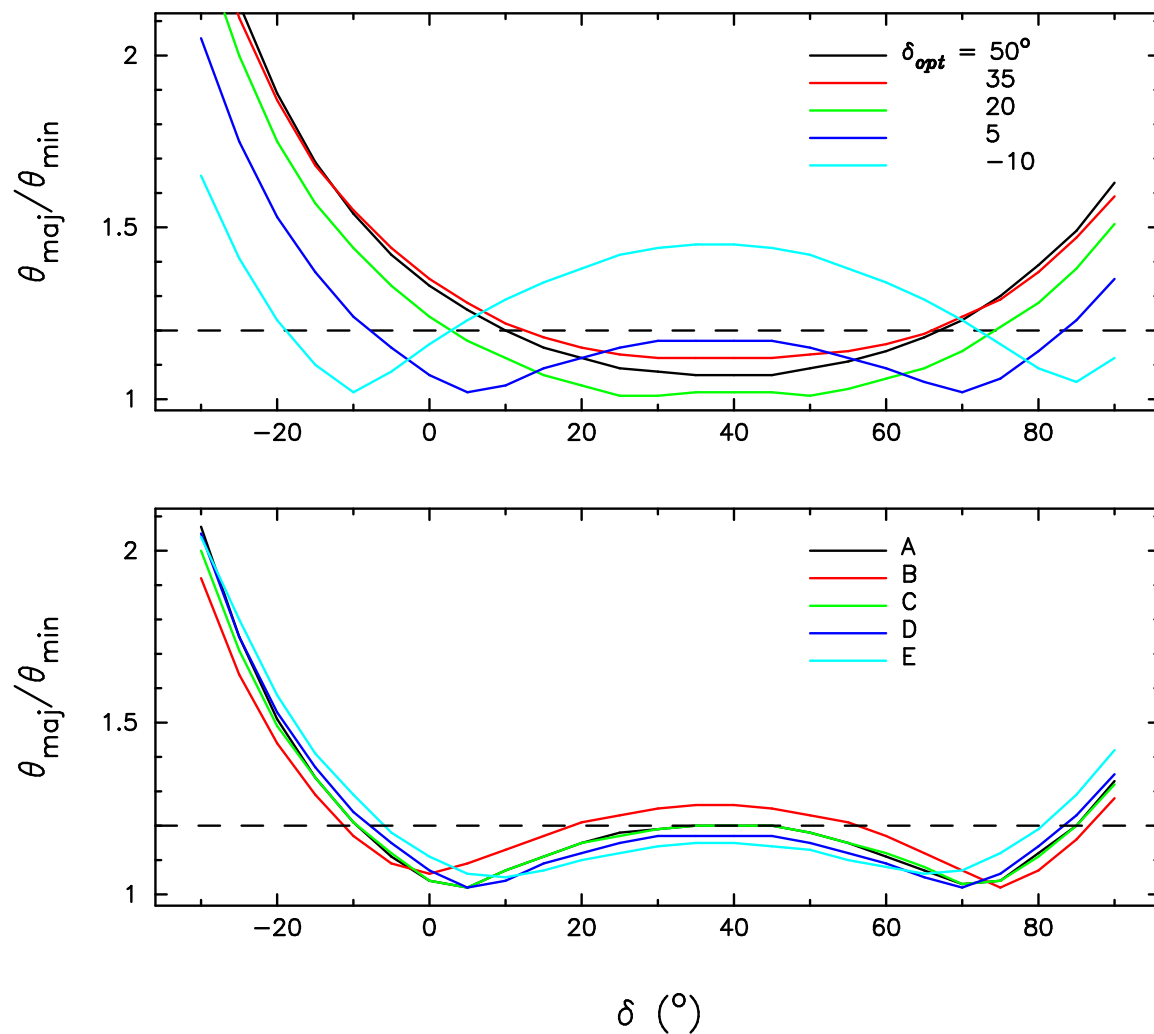


Fig. 1.— (top) Beam elongations as a function of source declination, with arrays at a site latitude of 37° optimized for source declinations of $\delta_{\text{opt}} = 50, 35, 20, 5, -10^\circ$ (shown as different colors). All elongations were calculated for ± 2 -hour tracks. (bottom) Beam elongations of the Version 2 Cedar Flat arrays as a function of source declination. For all arrays, the beam elongation is less than roughly 20% (dashed line) for declinations from about -10° to $+80^\circ$. Shaded visibilities have been flagged from the E array calculations where appropriate ($\delta < 0^\circ$).

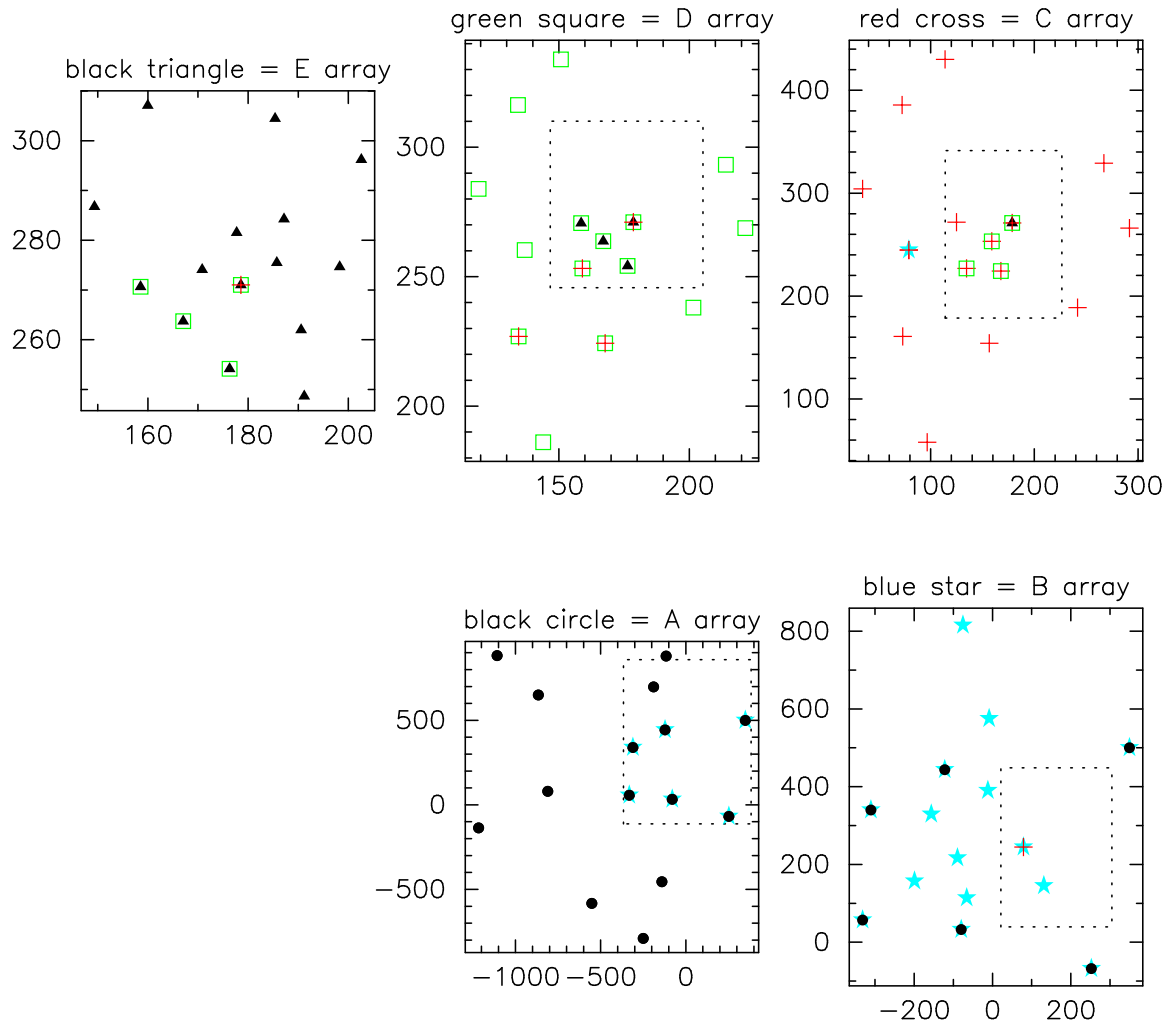


Fig. 2.— CARMA configurations. The abscissa (ordinate) is east (north) coordinates in meters. The dotted rectangles represent the outline of the next-smallest configuration. Shared stations are indicated by multiple symbols.

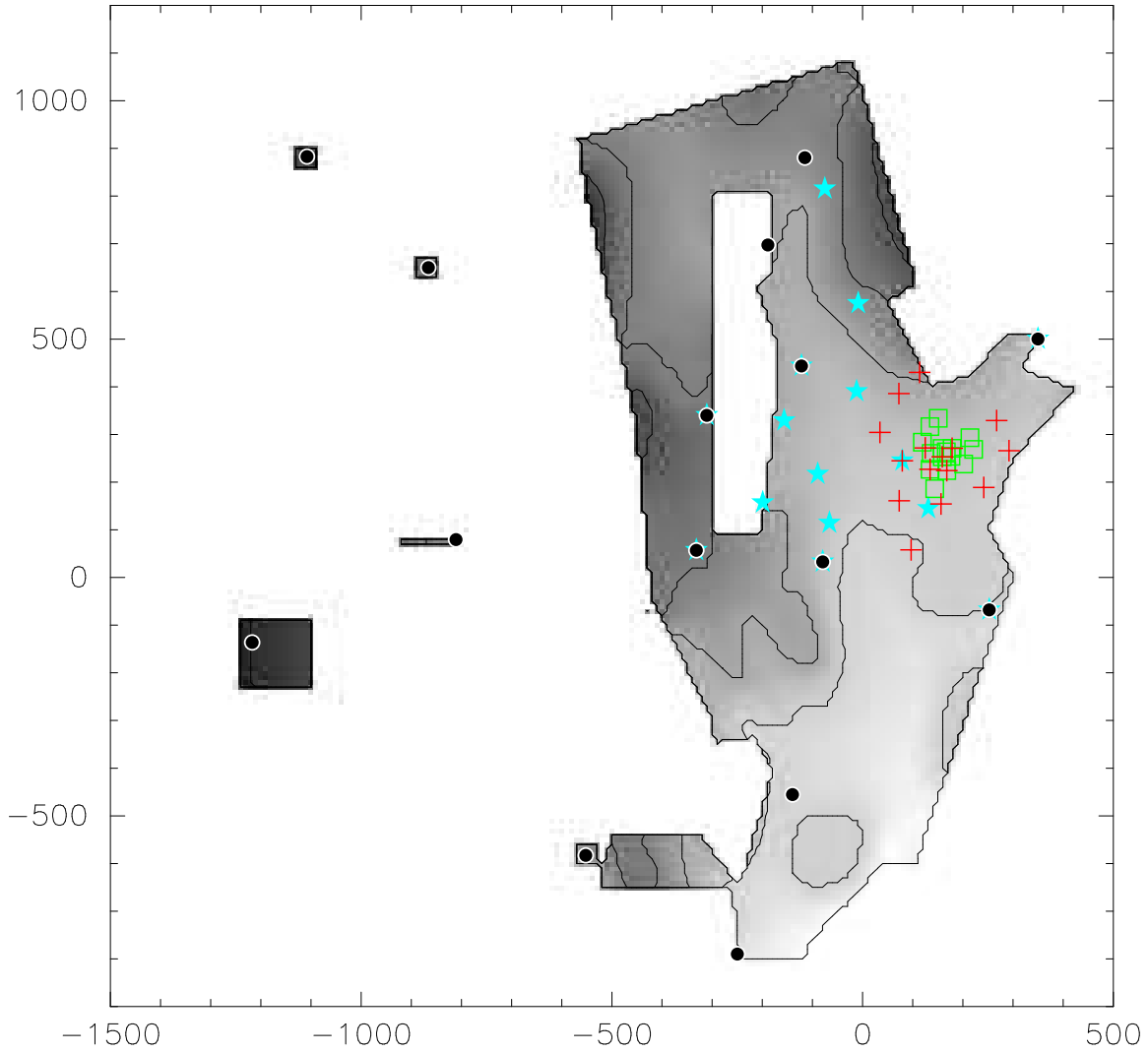


Fig. 3.— A, B, C, and D configurations overlaid on the site, shown with a mask used to exclude Rte. 168 and difficult terrain. Symbols are as in Figure 2. The abscissa (ordinate) is east (north) coordinates in meters.

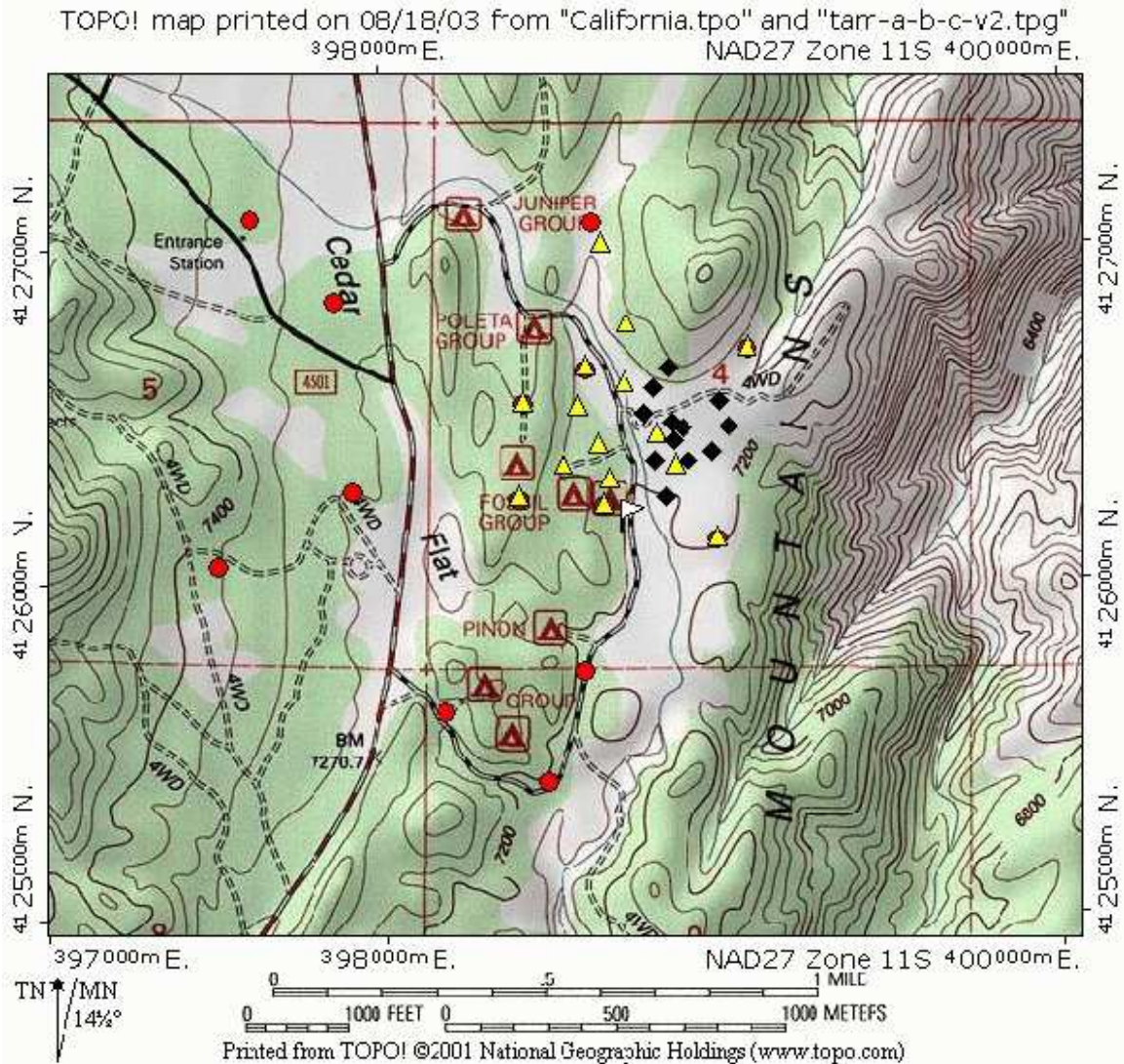


Fig. 4.— A (red circles), B (yellow triangles), and C (black diamonds) array stations, overlaid on a topographical map of the Cedar site. (At the resolution of the map, some of the C array stations are blended together.) The white flag points to the (0,0) reference position shown in Figures 2 and 3.

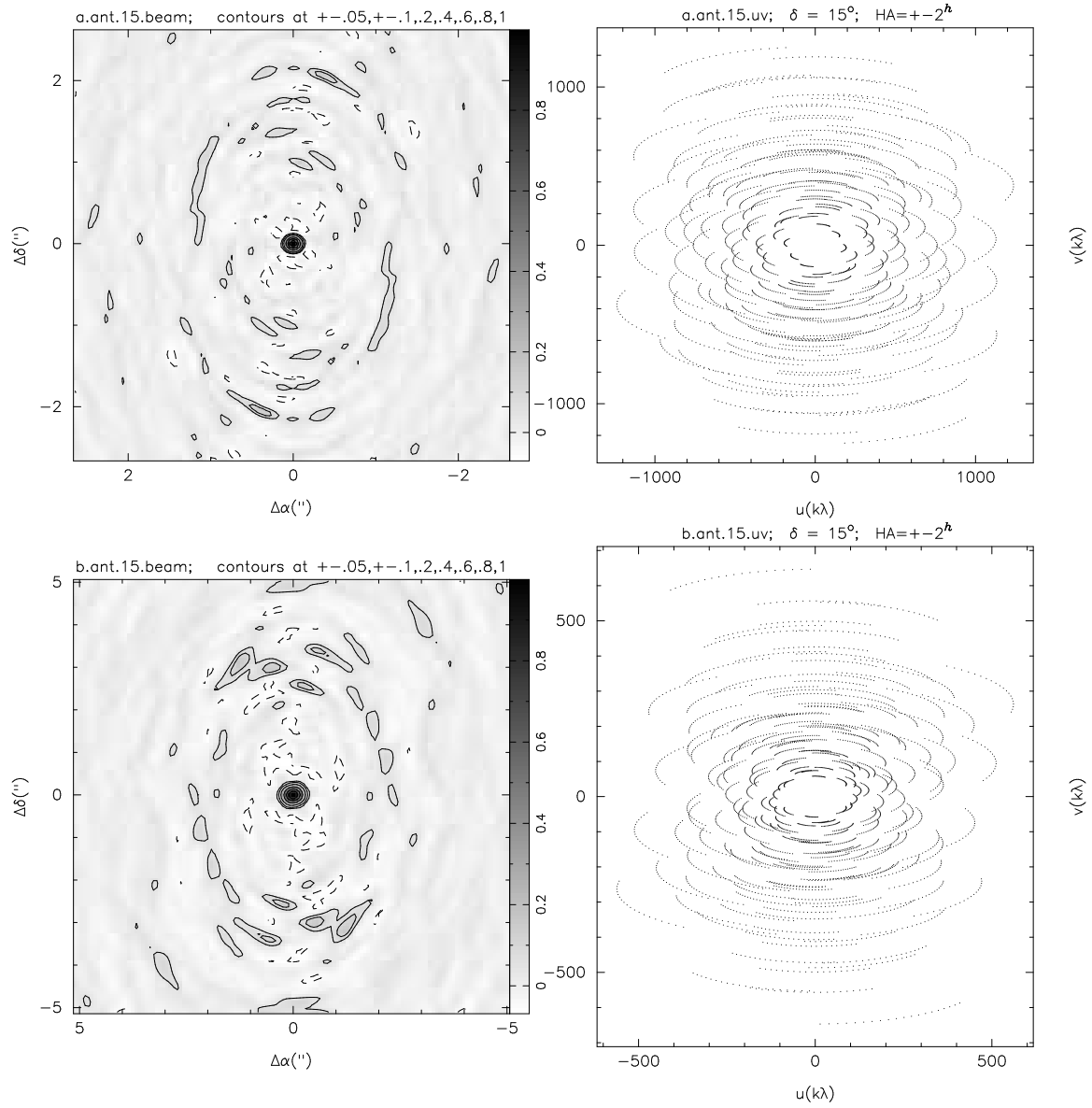


Fig. 5.— Naturally weighted beams (left column) and uv coverages (right column) for ± 2 -hour tracks run at $\nu=230$ GHz and $\delta=15^\circ$, for A array (top row) and B array (bottom row). Contours are listed at the top of the beam plots.

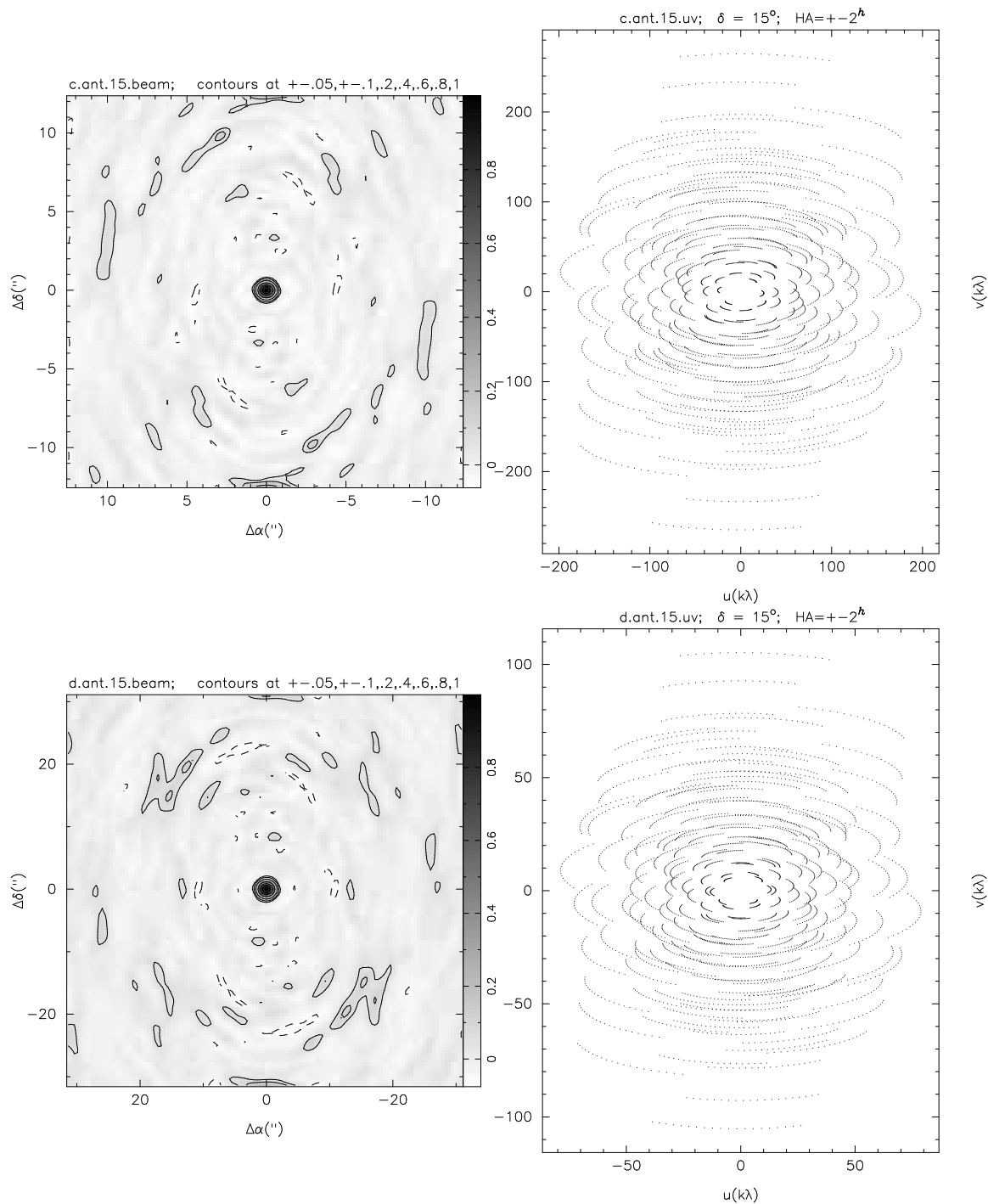


Fig. 5–cont.— Naturally weighted beams (left column) and uv coverages (right column) for ± 2 -hour tracks run at $\nu=230$ GHz and $\delta=15^\circ$, for C array (top row) and D array (bottom row). Contours are listed at the top of the beam plots.

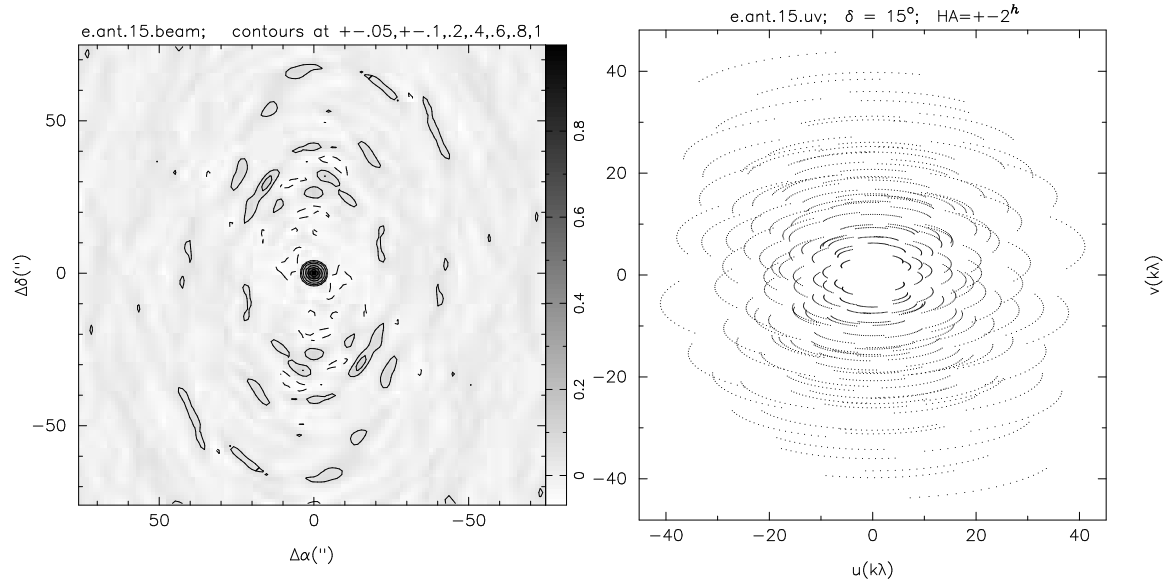


Fig. 5–cont.— Naturally weighted beams (left column) and uv coverages (right column) for ± 2 -hour tracks run at $\nu=230$ GHz and $\delta=15^{\circ}$, for E array. Contours are listed at the top of the beam plots.

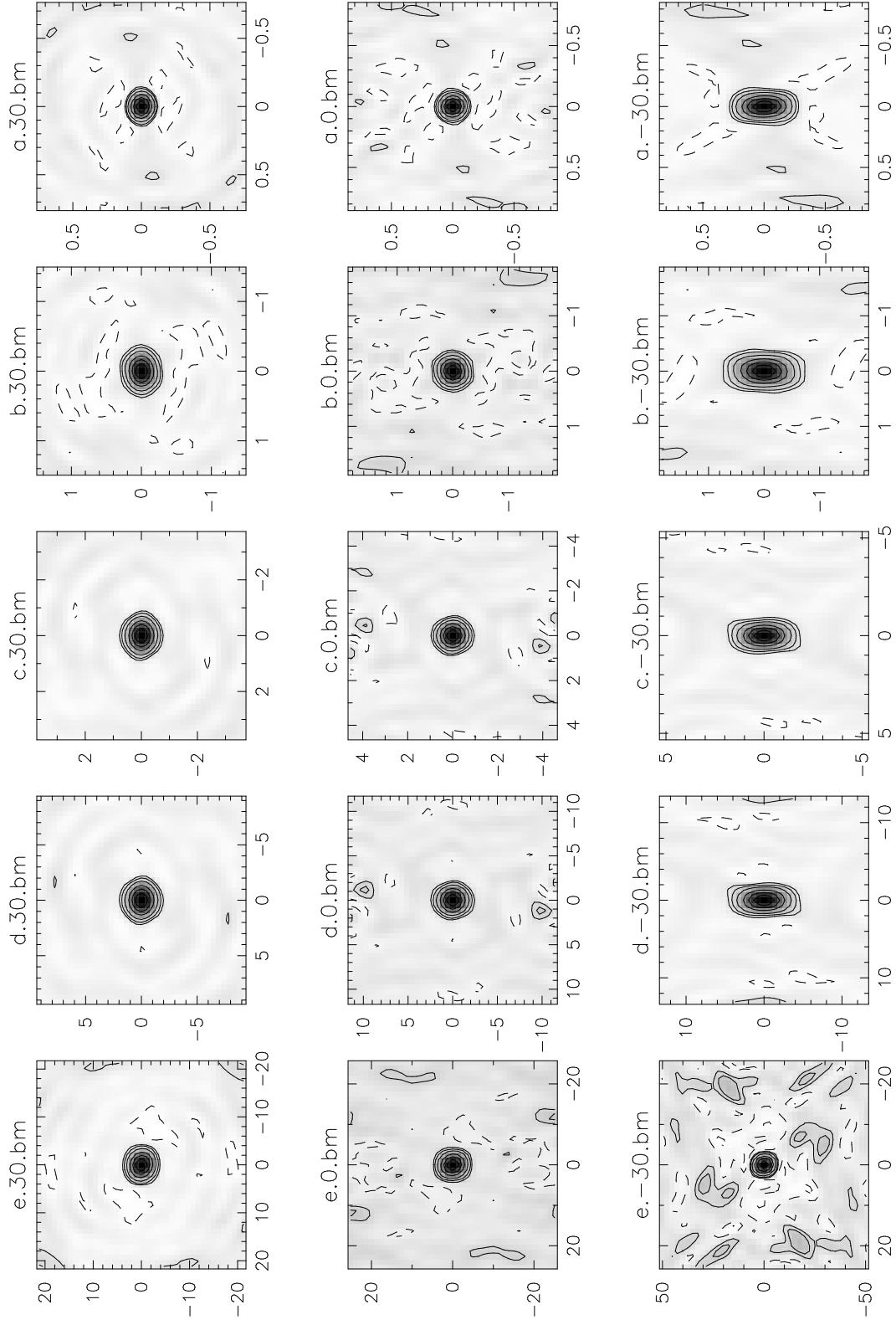


Fig. 6.— Inner portions of the naturally weighted beams for A-E arrays at $\delta = +30, 0, -30^\circ$. All beams were generated using ± 2 -hour tracks run at $\nu=230$ GHz. Contours are at $\pm 0.05, \pm 0.1, \pm 0.2, \pm 0.4, \pm 0.6, \pm 0.8, \pm 1$. Shaded data are flagged where appropriate ($\delta = -30^\circ$ for E and D arrays). Axes are $\Delta\alpha, \Delta\delta$ in arcsecond offsets.

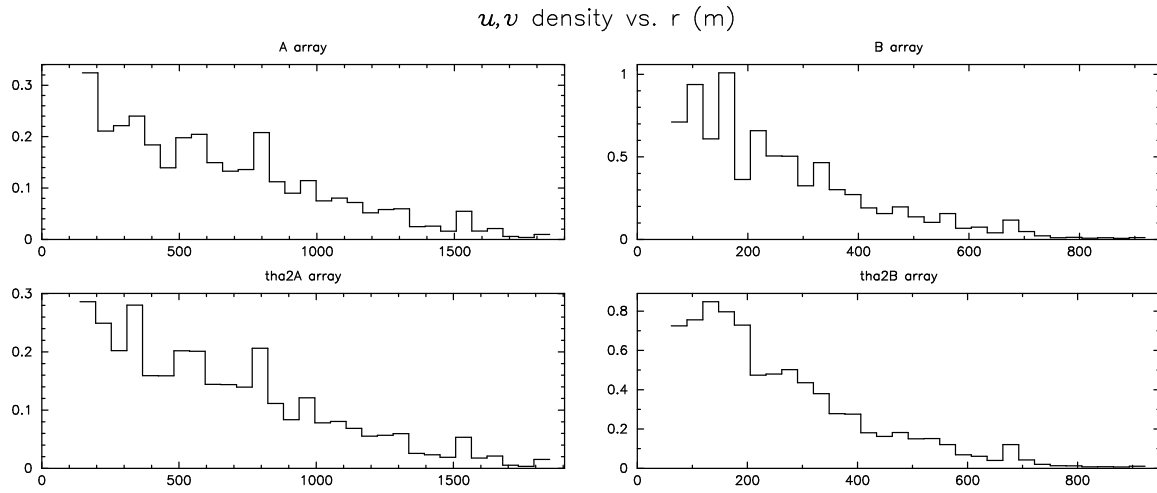


Fig. 7.— Histograms of uv density as a function of radius for the different arrays.

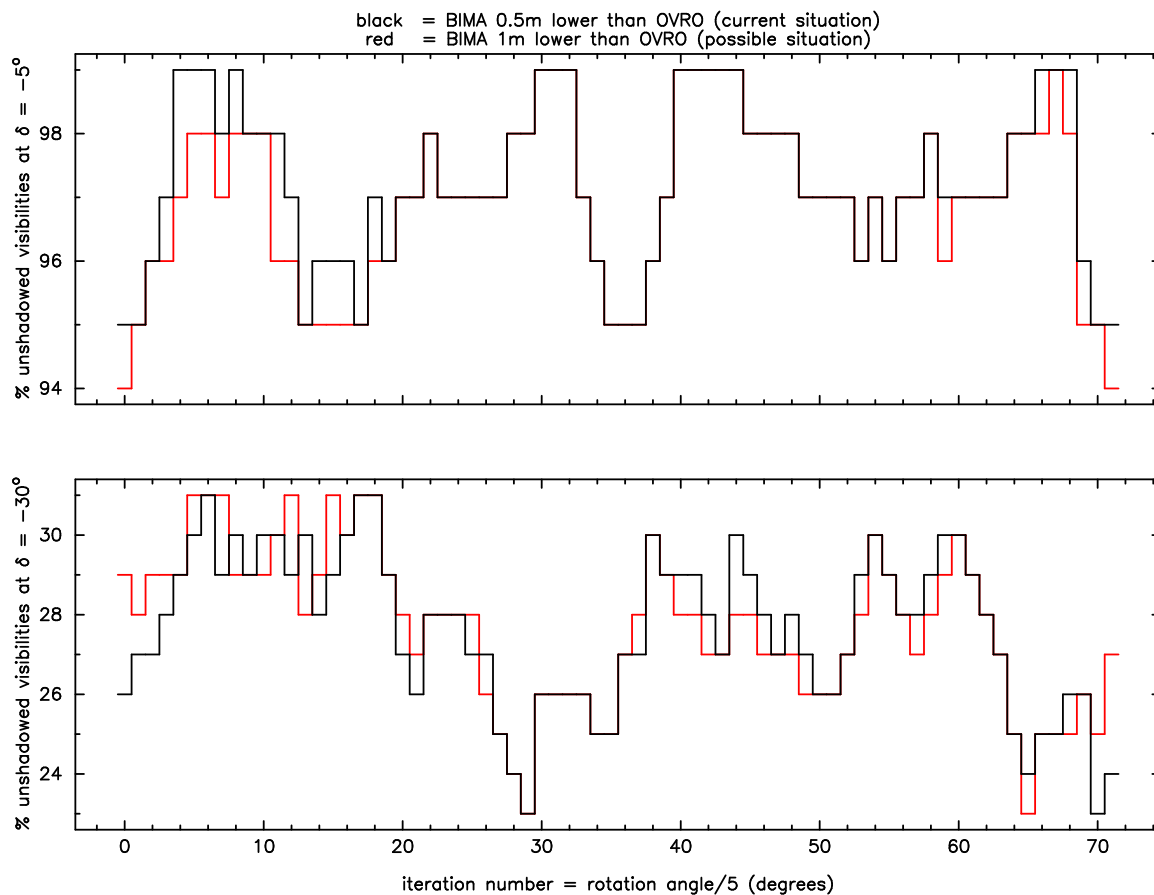


Fig. 8.— Shadowing as a function of E array rotation, for the case of 4-hour tracks centered on transit. The top panel represents the percentage of unshadowed visibilities at $\delta = -5^\circ$, while the bottom panel is at $\delta = -30^\circ$. The different color curves show the calculation run for different relative heights of the BIMA and OVRO elevation axes, as labeled at the top of the plot.

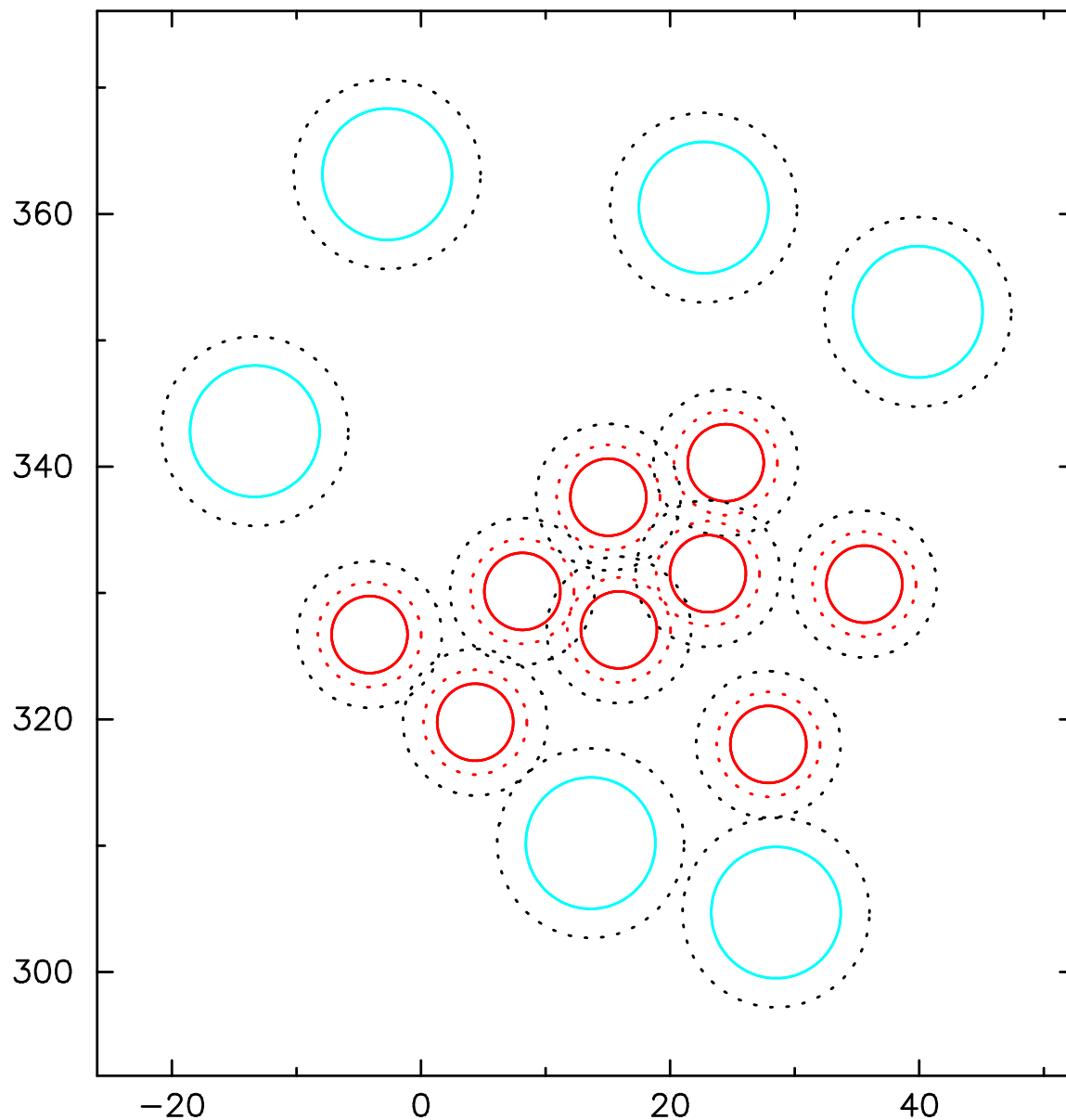


Fig. 9.— CARMA E array, shown with the placements of the two kinds of antennas. The abscissa (ordinate) is east (north) coordinates in meters. The 10.4m diameter of the OVRO antennas are shown as blue circles; the black dashed circles around the OVRO dishes are 15m in diameter, which is the collision-avoidance limit. The 6.1m diameter BIMA dishes are shown as solid red circles. The dashed red circles show the 8.3m closest-approach limit between BIMA dishes, which require collision avoidance hardware/software to implement (as is currently done at BIMA). The dashed black circles represent the 11.6m collision-avoidance limit for the BIMA dishes.